J Polym Res (2013) 20:114
DOI 10.1007/s10965-013-0114-8

ORIGINAL PAPER

Nanocomposites of polybenzoxazine and exfoliated montmorillonite using a polyhedral oligomeric silsesquioxane surfactant and click chemistry

Hui-Wang Cui · Shiao-Wei Kuo

Received: 12 December 2012 / Accepted: 20 February 2013 / Published online: 22 March 2013

Abstract In this study, an exfoliated montmorillonite was introduced into a benzoxazine matrix—prepared from paraformaldehyde, aniline, and phenol—to form polymer/exfoliated clay nanocomposites. Wide-angle X-ray diffraction, differential scanning calorimetry, dynamic mechanical analysis, thermogravimetric analysis, transmission electron microscopy, and contact angle measurements revealed the structures and thermal and mechanical properties of these polybenzoxazine/clay nanocomposites; the montmorillonite was exfoliated into nanoparticles (single sheets or layers) that were dispersed in the polybenzoxazine matrix. The incorporation of the exfoliated montmorillonite improved the polymer's glass transition and thermal decomposition temperatures, mechanical properties, and surface hydrophobicity.

Keywords Nanocomposites · Benzoxazine · POSS · Thermal properties

Introduction

Benzoxazine derivatives—characterized by an oxazine ring (a six-membered heterocycle containing oxygen and nitrogen atoms) attached to a benzene ring—are readily synthesized from a combination of a phenolic derivative, formaldehyde, and a primary amine. Depending on the positions of the heteroatoms, many benzoxazine structures can be prepared, including monomeric-type benzoxazines [1], main chain–type benzoxazines [2–6], side chain–type benzoxazines [7, 8], and telechelic-type benzoxazines [9]. Polybenzoxazines exhibit many unique properties: near-zero volume changes upon polymerization with high mechanical integrity [10]; low water absorption in water at room temperature [11]; surprisingly high glass transition temperatures (T_g) [12]; rapid development of their physical and mechanical properties during the polymerization process (e.g., 80 % of the T_g development occurs at a 50 % degree of conversion for a bisphenol-A/aniline–based benzoxazine) [13]; very high char yields [14]; and low surface energies [15, 16]. Therefore, polybenzoxazines have been studied widely ever since they were first reported [17], with various related applications also appearing gradually [18–23].

For further improve the physical properties of polymer matrix, one of the most important technologies is the manufacture of (nano)composites through blending with other polymers or nanofillers [24–26]; for example, reinforcement with glass fibers [27], cellulose fibers [28], or carbon fibers [29] or the incorporation of nanofillers from clay [30–34], carbon nanotubes [35, 36], and polyhedral oligomeric silsesquioxane (POSS) [37–48]. These (nano)composites can impart polybenzoxazines with excellent processability and superb mechanical properties, without forming volatile species. Although many reports describe nanocomposites manufactured through the incorporation of clay into polybenzoxazines, in those cases the clays were merely intercalated and dispersed in the polymeric matrix with a layered or lamellar structure [30–34]. In this present study, we used POSS nanocomposites to improve the exfoliation of clay incorporated in a polybenzoxazine. After intercalating propargyl dimethylstearylammonium bromide between the layers of montmorillonite (MMT) to form intercalated montmorillonite (In-MMT), we introduced a monofunctionalized azide-POSS derivative to undergo Huisgen [2+3] cycloadditions (click reactions) with the acetylenic intercalator units, resulting in the MMT exfoliating into nanoparticles in the form of single sheets or layers [48].

H.-W. Cui · S.-W. Kuo (✉)
Department of Materials and Optoelectronic Science,
Center for Nanoscience and Nanotechnology,
National Sun Yat-Sen University, Kaohsiung 804, Taiwan
e-mail: kuosw@mail.nsysu.edu.tw

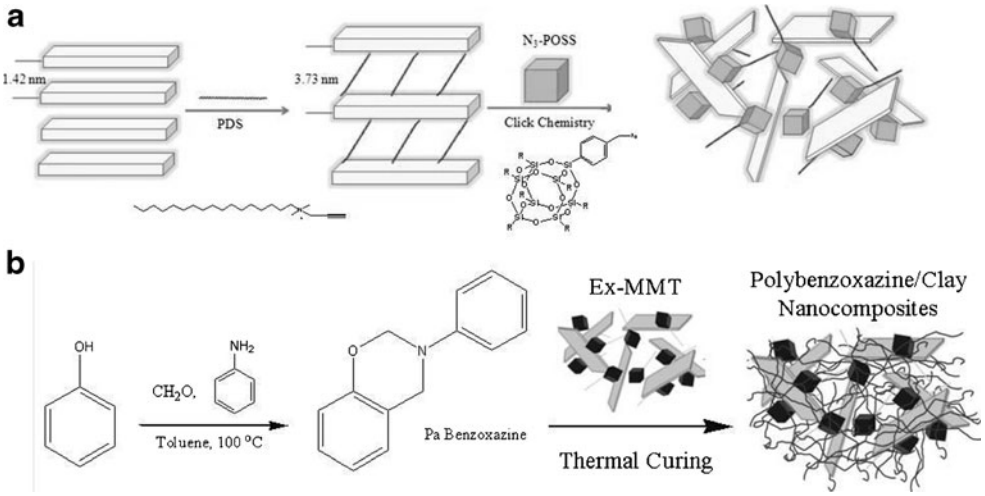

Scheme 1 **a** The preparation of exfoliation MMT by using click reaction and **b** preparation of exfoliated nanocomposites from benzoxazine and exfoliation MMT from (a)

We then incorporated this exfoliated montmorillonite (Ex-MMT) into the Pa-type benzoxazine (3-phenyl-3,4-dihydro-2H-benzoxazine) monomer-derived from paraformaldehyde, aniline, and phenol-to form exfoliated polybenzoxazine nanocomposites (Scheme 1), the thermal and surface properties and morphologies of which we investigated using wide-angle X-ray diffraction (WAXD), differential scanning calorimetry (DSC), dynamic mechanical analysis (DMA), thermogravimetric analysis (TGA), transmission electron microscopy (TEM), and contact angle analyses.

Experiments

Samples

Montmorillonite (MMT) was purchased from Nanocor (USA); N,N-dimethylstearylamine, propargyl bromide, paraformaldehyde, and aniline were obtained from Tokyo Chemical Industry; N,N-dimethylformamide (DMF), sodium azide (NaN_3), ethanol, vinylbenzyl chloride, and N,N,N,N,N-pentamethyldiethylenetriamine (PMDETA) were purchased from Sigma–Aldrich. Copper(I) bromide (CuBr, Alfa Aesar, USA) was purified through washing with glacial AcOH overnight, followed by washing with absolute ethyl ether and drying under vacuum. All solvents were distilled prior to use. The mono-functionalized azide-POSS derivative [49–53] and the Pa monomer 3-phenyl-2H,4H-benzoxazine [19] were prepared according to previously reported procedures. In-MMT was prepared as follows: A mixture of N,N-dimethylstearylamine (3.86 g, 130 mmol) and propargyl bromide (1.55 g, 130 mmol) in distilled water (100 mL) and EtOH (100 mL) was heated at 80 °C for 0.5 h with rapid stirring to form propargyldimethylstearylammonium bromide; MMT (10 g) was added to the solution, which was then stirred vigorously for 4 h; after cooling to room temperature, washing, filtering, drying, and grinding, In-MMT was obtained. Ex-MMT was prepared from In-MMT, the mono-functionalized azide-POSS derivative, and click reactions as follows: Mono-functionalized azide POSS (N_3-POSS, 0.589 g, 0.500 mmol), In-MMT (0.521 g), and CuBr (0.0717 g, 0.500 mmol) were mixed together in the solid state under vacuum; after adding anhydrous DMF (50 mL), the mixture was stirred rapidly for 12 h under vacuum; next, six freeze/thaw/pump cycles were performed, with the total time of freezing and pumping being 0.5 h and the time of the thaw, while strongly stirring, being 1 h in each cycle; at this point, N,N,N,N,N-pentamethyldiethylenetriamine (0.100 mL, 0.500 mmol) was added and one freeze/thaw/pump cycle was performed again; after the final thaw to room temperature, the reaction mixture was stirred rapidly for 12 h under vacuum; after washing sequentially with anhydrous DMF and distilled water, filtering, drying, and grinding, Ex-MMT was obtained.

Table 1 Compositions of polybenzoxazine/clay nanocomposites

	BM	BIM	BEM-A	BEM-B	BEM-C	BEM-D	BEM-E	BEM-F	BEM-G
Pa	5 g	5 g	5 g	5 g	5 g	5 g	5 g	5 g	5 g
MMT	0.25 g	—	—	—	—	—	—	—	—
In-MMT	—	0.25 g	—	—	—	—	—	—	—
Ex-MMT	—	—	0.05 g	0.15 g	0.25 g	0.35 g	0.50 g	1.50 g	2.50 g

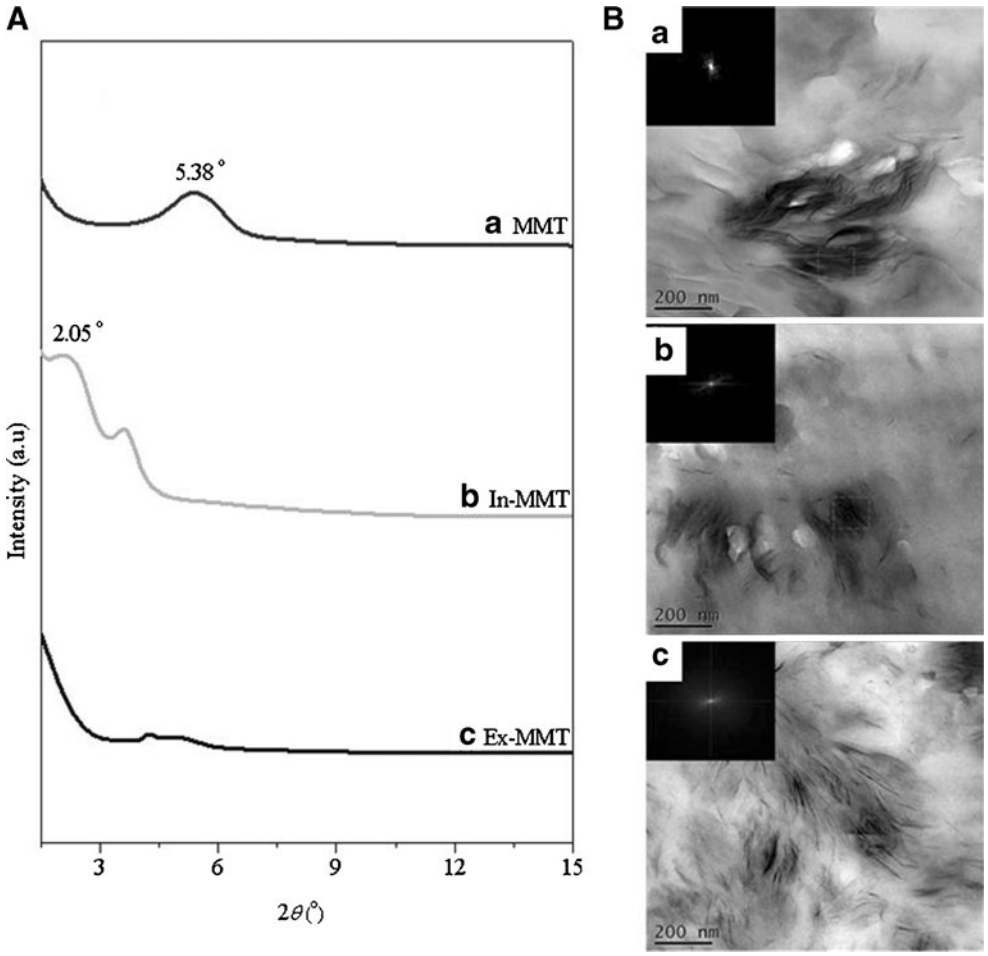

Fig. 1 **a** XRD patterns and **b** TEM images of **a** MMT, **b** In-MMT, and **c** Ex-MMT

Polybenzoxazine/clay nanocomposites

Pa-Type benzoxazine monomer was mixed with MMT, In-MMT, or Ex-MMT with vigorously stirring until the sample became homogeneous. The sample was then placed in a natural oven and cured at 140 °C for 3 h, 160 °C for 3 h, and then 200 °C for 4 h under a heating rate of 2 °C·min^{-1}. BM was formed from Pa and MMT; BIM from Pa and In-MMT; and BEM from Pa and Ex-MMT (Table 1). The weight ratio of MMT or In-MMT to Pa was fixed at 5 wt%; those of Ex-MMT to Pa were 1, 3, 5, 7, 10, 30, and 50 wt%, named BEM-A, BEM-B, BEM-C, BEM-D, BEM-E, BEM-F, and BEM-G, respectively.

Characterization

WAXD data were collected using a BL17A1 wiggler beam line at the National Synchrotron Radiation Research Center (NSRRC), Taiwan. A triangular bent Si (111) single crystal was employed to obtain a monochromated beam having a wavelength (λ) of

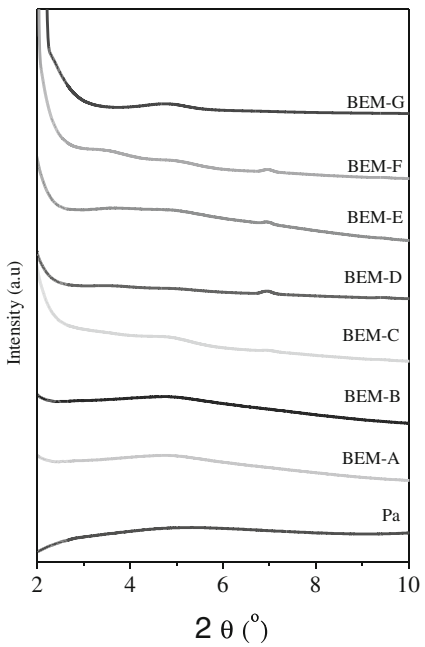

Fig. 2 XRD patterns of Pa benzoxazine samples containing various contents of Ex-MMT

1.33001 Å. Values of $d_{(001)}$ were calculated using Bragg's law, $\lambda=2d\sin\theta$, where λ is the wavelength of the X-ray radiation, d is the distance between two MMT layers, and θ is the diffraction angle. TEM images were recorded using a JEOL-2100 transmission electron microscope operated at an accelerating voltage of 200 kV. Ultrathin sections (thickness: ca. 70 nm) of the TEM samples were prepared using a Leica Ultracut UCT microtome equipped with a diamond knife; they were placed onto Cu grids coated with carbon-supporting films. The glass transitions of the samples were studied using a TA Q-20 differential scanning calorimeter operated under an atmosphere of pure N_2. The sample (ca. 7 mg) was placed in a sealed aluminum sample pan. The glass transition scans were conducted from 25 to 250 °C at a rate of 20 °C·min^{-1}. The thermal stabilities of the samples were measured using a TA Q-50 thermogravimetric analyzer operated under an atmosphere of pure N_2. The sample (ca. 7 mg) was placed in a Pt cell and heated at a rate of 20 °C·min^{-1} from 30 to 800 °C under a N_2 flow rate of 60 mL·min^{-1}. The dynamic mechanical properties of the samples were investigated using a PerkinElmer DMA800 dynamic mechanical analyzer operated in air. The sample (10 mm × 8 mm × 2 mm) was fixed on the bracket and subjected to the single-frequency/strain mode as the temperature was increased from 25 to 200 °C at a rate of 2 °C·min^{-1}. A Dataphysics OCA contact angle system was used to measure the advancing contact angles on the samples (10 mm×8 mm×2 mm) at 25 °C; a drop (5 μL) of distilled water, ethylene glycol (EG), or diiodomethane (Diio) was placed onto the sample surface using a syringe.

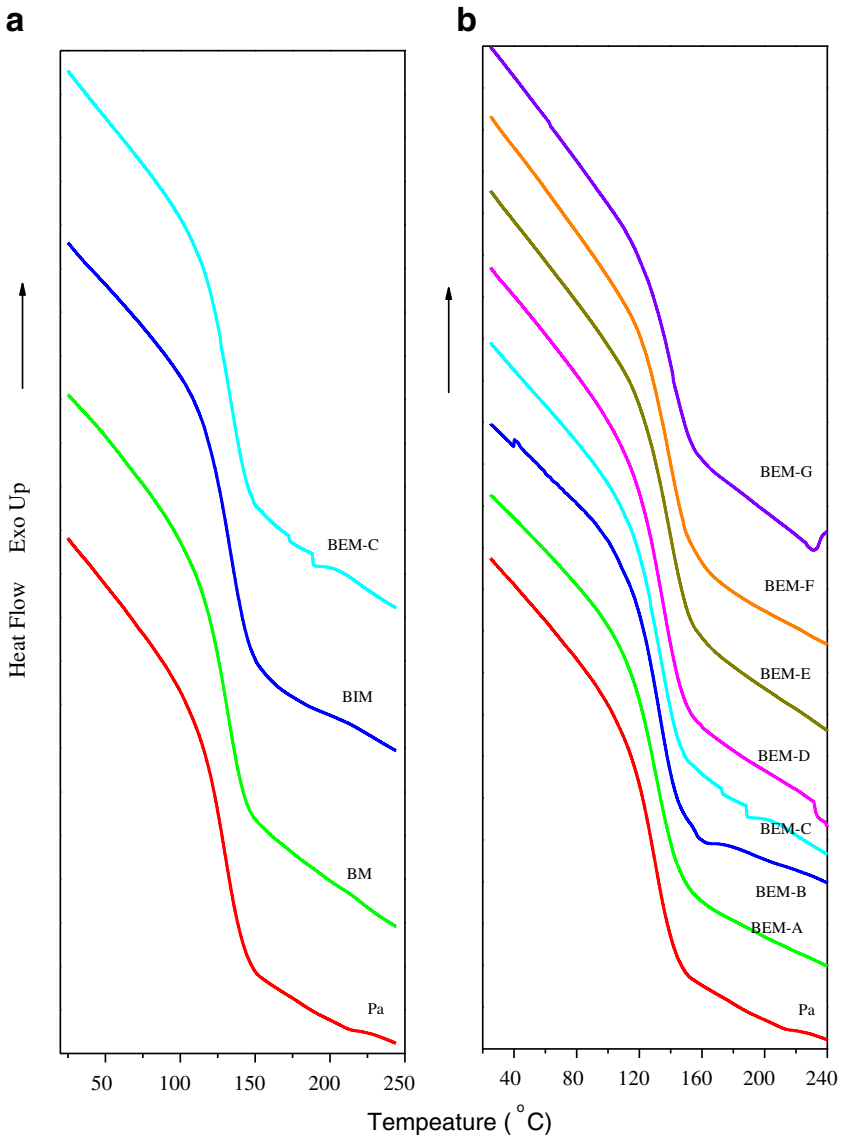

Fig. 3 DSC curves of (**a**) Pa, BM, BIM, and BEM-C and (**b**) Pa benzoxazine samples containing various contents of Ex-MMT (BEM)

Results and discussion

Figure 1(A)-(a) displays the XRD pattern of In-MMT; its diffraction peak appeared at a value of 2θ of 2.05°, providing a value of $d_{(001)}$ of 3.73 nm. For pure MMT, these values were 5.38° and 1.42 nm, respectively [Fig. 1(A)-(b)]. The greater value of $d_{(001)}$ for In-MMT reveals that propargyl dimethylstearylammonium bromide had indeed intercalated between the layers of MMT, opening them to a certain extent. In contrast, we observed no diffraction peak in the 2θ range from 0.5 to 5° in the XRD pattern of Ex-MMT [Fig. 1(A)-(c)], which we had prepared through click reactions between In-MMT and the mono-functionalized azide-POSS derivative. During this transformation, the POSS nanoparticles had to enter between the layers of In-MMT to undergo click reactions with the intercalated propargyldimethylstearylammonium bromide. The entry of the cage-like POSS nanoparticles led to partial exfoliation of MMT into nanoparticles having the form of single sheets or layers; the click reactions had a further and stronger exfoliating effect, causing the MMT to undergo complete exfoliation [Fig. 1(B)-(c)]. [47]

Next, we incorporated the Ex-MMT at different weight ratios into the polybenzoxazine matrix formed from the Pa monomer, obtaining samples BEM-A, BEM-B, BEM-C, BEM-D, BEM-E, BEM-F, and BEM-G (Table 1). For comparison, we also prepared MMT-based polybenzoxazine nanocomposites incorporating BM and In-MMT (Table 1). Figure 2 reveals that the XRD patterns of samples BEM-A to BEM-G featured no diffraction peaks in the 2θ range of 0.5–5°, indicating that each contained fully exfoliated nanocomposites. The dispersion of exfoliated MMT sheets or layers in the polybenzoxazine matrix had a significant effect on the thermal properties of these systems; we investigated the glass transition temperatures, thermal degradation behavior, and mechanical properties using DSC, DMA, and TGA, respectively.

Figure 3(a) displays the DSC traces of pure Pa and BM, BIM, and BEM-C having the same fixed ratio (5 wt%) of MMT, In-MMT, and Ex-MMT, respectively, in the polybenzoxazine matrix; their values of T_g were 129, 131, 133, and 134 °C, respectively. In the DSC traces of Pa featuring contents of Ex-MMT ranging from 1 to 50 wt% [Fig. 3(b)], the values of T_g increased upon increasing the Ex-MMT content; Table 2 summarizes the results. Figs. 4(a) and (b) display DMA data for pure Pa, BM, BIM, and BEM-C; each of the samples exhibited a high storage modulus (ca. 5.00×10^9 Pa) at temperatures below its glass transition, at which the polymeric chains and segments were frozen and could not move. Deformation arises mainly from changes to the lengths and angles of the chemical bonds between the atoms in the polymeric chains and segments. In the glass state, these polymeric materials exhibited great elasticity, high storage moduli, and low loss moduli. Moreover, the incorporation of MMT or In-MMT into the polybenzoxazine did not improve the storage modulus, due to the poor dispersion of the MMT species; in contrast, the storage modulus after incorporating a certain content of Ex-MMT into polybenzoxazine was slighter higher than that of pure polybenzoxazine, probably because of the exfoliation of this clay in the polymer matrix. In addition, the presence of MMT, In-MMT, and Ex-MMT influenced the values of T_g

Table 2 Thermal properties and surface hydrophobicities of pure Pa and the nanocomposites Pa with pure MMT (BM), Pa with In-MMT (BIM), and Pa with Ex-MMT (BEM)

	T_g[a]	T_g[b]	Char Yield[c]	T_d[c] (°C)		Derivative Weight (%·°C^{-1})[c]		Contact Angle (°)		
	(°C)	(°C)	(%)	95 %	50 %	Peak 1	Peak 2	Water	EG	Diio
Pa	130	129	35.3	349	485	0.40	0.43	96.7	70.6	50.3
BM	135	131	39.3	357	498	0.38	0.37	97.6	71.4	51.9
BIM	137	133	37.0	347	486	0.36	0.41	98.2	72.5	53.2
BEM-A	134	132	37.0	353	494	0.37	0.42	102.7	75.0	53.0
BEM-B	136	132	37.0	352	495	0.36	0.41	103.7	75.8	58.6
BEM-C	140	134	38.6	345	496	0.34	0.39	104.5	76.4	60.1
BEM-D	143	136	39.8	350	501	0.32	0.39	105.2	77.0	64.1
BEM-E	145	140	40.5	348	503	0.32	0.39	106.1	77.5	67.7
BEM-F	—	141	41.2	347	506	0.32	0.36	—	—	—
BEM-G	—	144	45.7	347	546	0.29	0.31	—	—	—

[a] Determined through DMA

[b] Determined through DSC

[c] Determined through TGA; the values of T_d were determined at weight percentages of 95 and 50 % in Figs. 4(a) and (c); the Derivative Weights were the values at Peaks 1 and 2 marked in Figs. 4(b) and (d)

of the polybenzoxazine. In this study, we determined values of T_g from the loss modulus peak [Figs. 4(b) and (d)]. Figure 4 and Table 2 reveal that, at a same fixed ratio (5 wt%) of MMT, In-MMT, and Ex-MMT relative to Pa polybenzoxazine, the value of T_g increased from 129.7 °C for Pa to 135.4 °C for BM, 137.1 °C for BIM, and 139.5 °C for BEM-C, respectively, as a result of their different transfer modes for heat and mass. Scheme 2(a) illustrates how the heat flow could pass through the polymeric chains and segments in Pa polybenzoxazine directly, allowing them to move freely and resulting in a sharp change of modulus and a rapid glass transition. The transfer paths for heat flow in BM, BIM, and BEM [Schemes 2(b)–(f)] were delayed, blocked, or distorted as a result of the incorporation of MMT, In-MMT, and Ex-MMT, respectively, into the polybenzoxazine matrix. These variations in the transfer paths of the heat flow caused the moduli of BM, BIM, and BEM to decrease slowly (or delayed their sharp changes); the same phenomenon occurred for the glass transition. Thus, the values of T_g of BM, BIM, and BEM were higher than that of Pa polybenzoxazine. Greater amounts of Ex-MMT in the polybenzoxazine matrix led to more-significant changes in the transfer paths of heat flow and, therefore, induced higher values of T_g; indeed, when the content of Ex-MMT was 1, 3, 5, 7, and 10 wt% relative to Pa polybenzoxazine, the values of T_g were 134, 136, 140, 143, and 145 °C, respectively. The glass transition temperatures we obtained through DMA followed a similar trend to those from our DSC analyses; the values of T_g obtained from the former were, however, higher than those

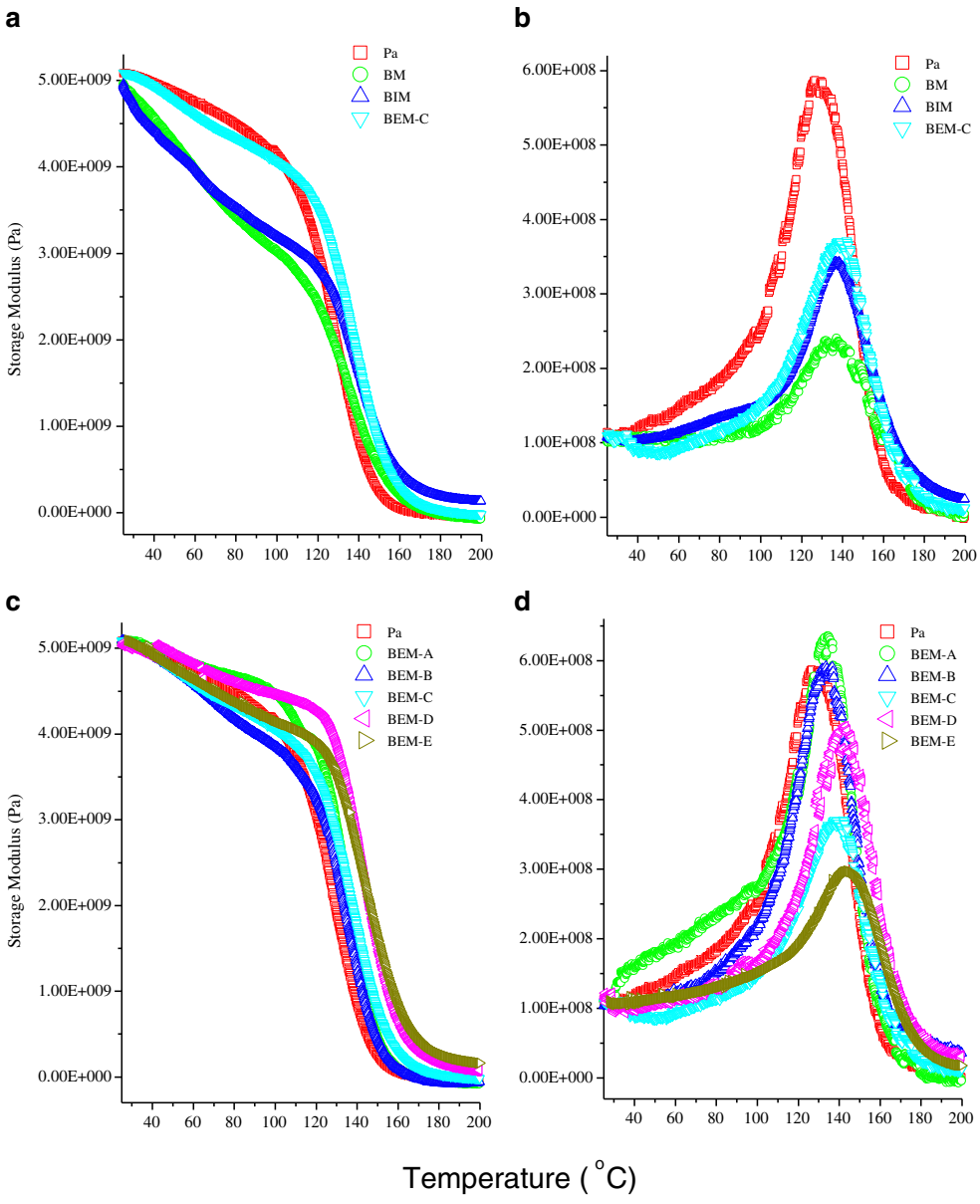

Fig. 4 DMA data revealing the (**a, c**) storage and (**b, d**) loss moduli of (**a, b**) Pa, BM, BIM, and BEM-C and (**c, d**) Pa benzoxazine samples containing various contents of Ex-MMT (BEM)

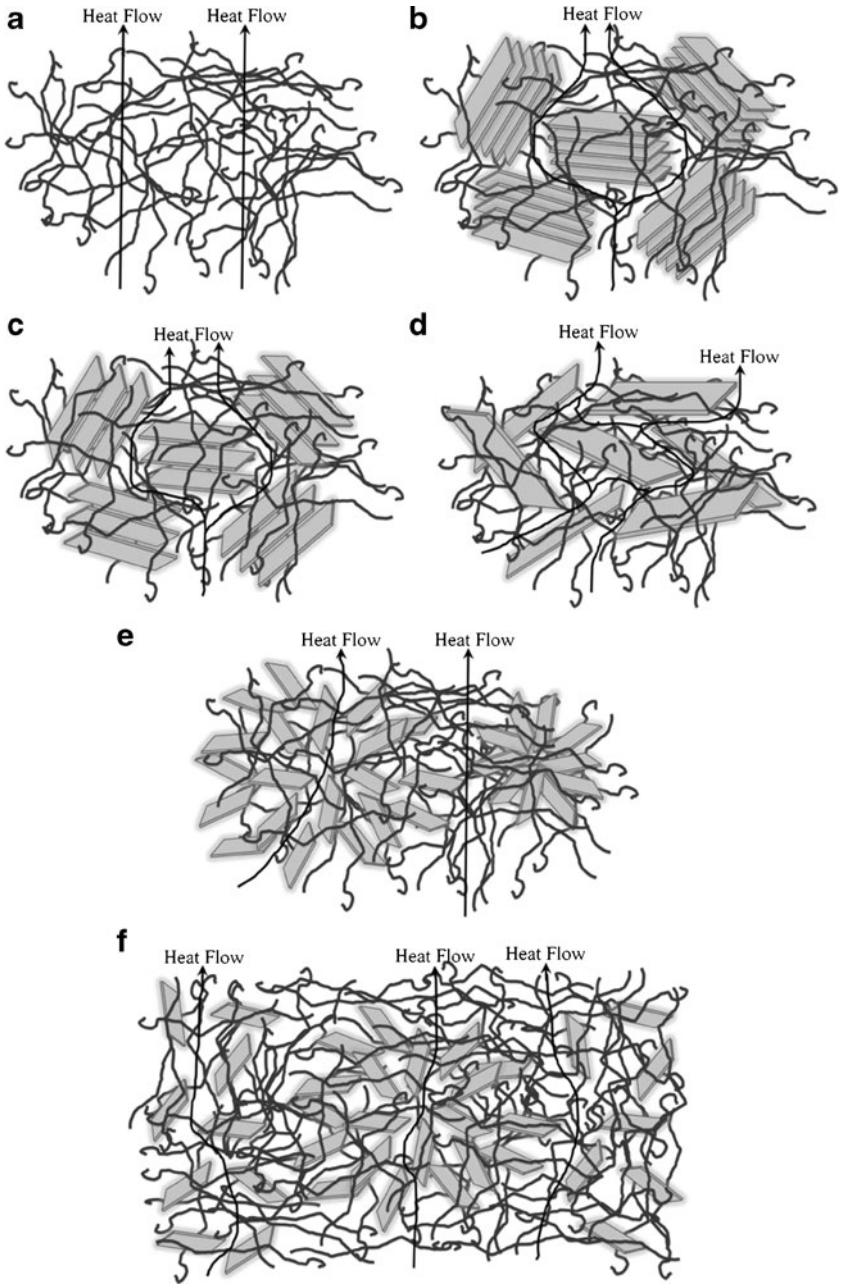

Scheme 2 Dispersion diagrams and corresponding heat flows for (**a**) Pa, (**b**) BM, (**c**) BIM, (**d**)–(**f**) BEM

from the latter, as would be expected because the molecules would have to move significantly to change the modulus by several orders of magnitude to undergo the glass transition. Therefore, the glass transitions obtained through DMA were delayed (i.e., higher temperatures) relative to those obtained through DSC.

Similarly, the incorporation of MMT, In-MMT, and Ex-MMT into the polybenzoxazine matrix and the resulting changes to the transfer paths of heat flow also influenced the thermal degradation significantly. Fig. 5(a) displays the TGA traces of pure Pa, BM, BIM, and BEM-C. The char yield of pure Pa was 35.4 wt%. Because of the presence of inorganic MMT, the char yield of BM increased to 39.4 wt%. Although the char yield of BIM at 37.1 wt% was higher than that of pure Pa, it was lower than that of BM because the organic intercalator, propargyldimethylstearylammonium bromide, had entered into the MMT layers. The char yield of BEM-C (38.62 %) was lower than that of BM, but higher than those of pure Pa and BIM, because of the click reactions that had occurred between the propargyl-containing intercalator and the mono-functionalized azide POSS in the MMT layers. Similar phenomena were manifest in the thermal degradation temperatures (T_d) and derivative weights. The values of T_d, defined as the temperature of 50 wt% weight loss, were 485 °C

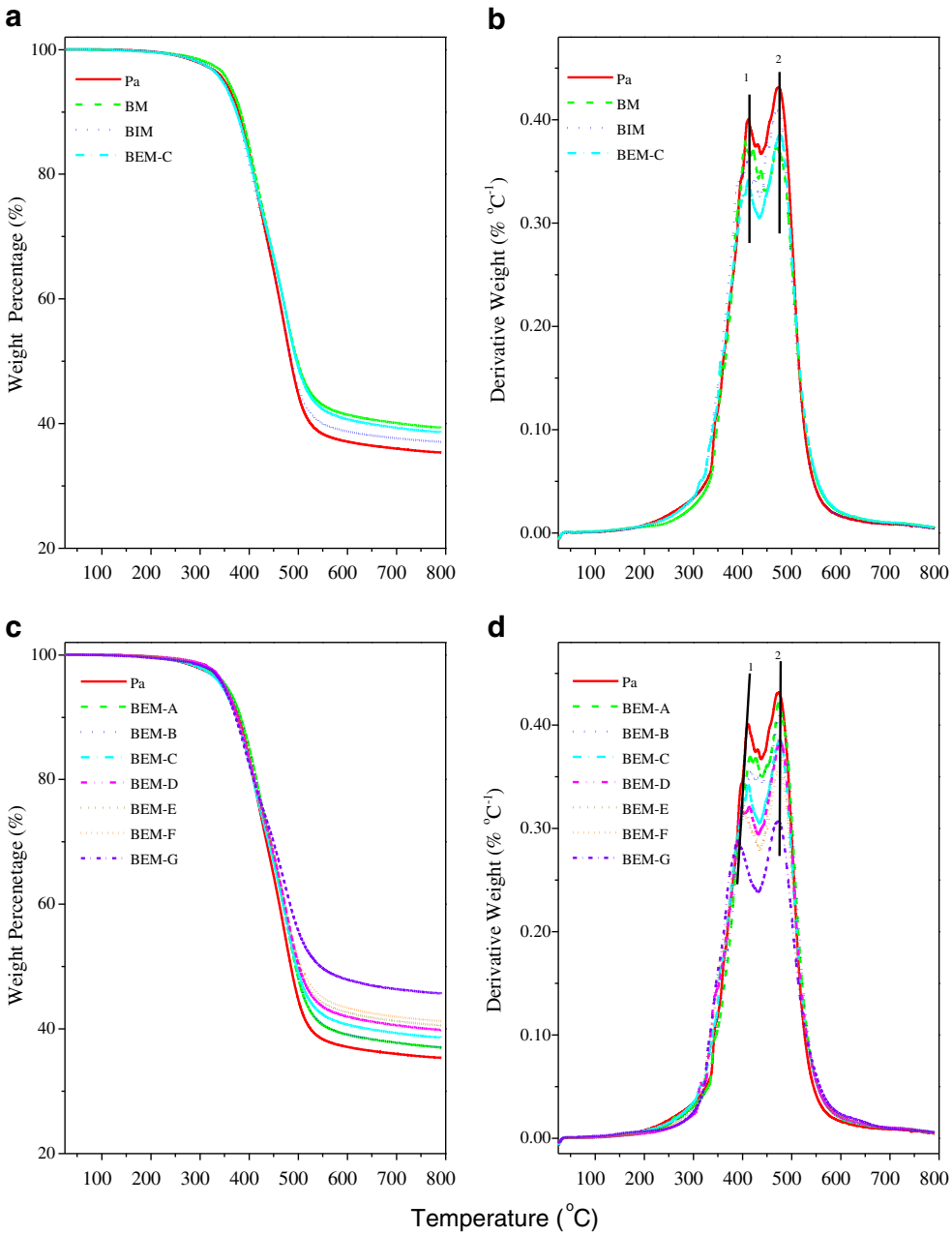

Fig. 5 TGA data revealing the (**a, c**) weight percentages and (**b, d**) derivative weights of (**a, b**) Pa, BM, BIM, and BEM-C and (**c, d**) Pa benzoxazine samples containing various contents of Ex-MMT (BEM)

for pure Pa, 498 °C for BM, 487 °C for BIM, and 497 °C for BEM-C. Thus, the presence of MMT, In-MMT, and Ex-MMT delayed the thermal degradation. The derivative weights [Fig. 5(b), Table 2] for pure Pa, BM, BIM, and BEM-C were 0.40, 0.38, 0.36, and 0.34 %·°C^{-1}, respectively, at peak 1 and 0.43, 0.37, 0.41, and 0.39 %·°C^{-1}, respectively, at peak 2. Thus, the incorporated MMT, In-MMT, and Ex-MMT changed the transfer paths of heat flow, influenced the char yield, delayed thermal degradation, and decreased the pyrolysis rate of the derivative weight. The effects of MMT, In-MMT, and Ex-MMT on the thermal degradation became increasingly significant upon increasing their contents. As indicated in Figs. 5(c) and (d) and Table 2, when we increased the content of Ex-MMT relative to Pa in BEM from 1 to 50 % (corresponding to BEM-A to BEM-G), the char yield and the value of T_d both increased while the derivative weights at peaks 1 and 2 both decreased, as expected. Although the values of T_d at a weight percentage of 95 % for Bz, BM, BIM, and BEM did not vary significantly, our findings described above are enough to prove the delaying effect on thermal degradation of polybenzoxazine caused by the presence of MMT, In-MMT, and Ex-MMT.

The glass transition and thermal degradation data for BM, BIM and BEM were closely related to their

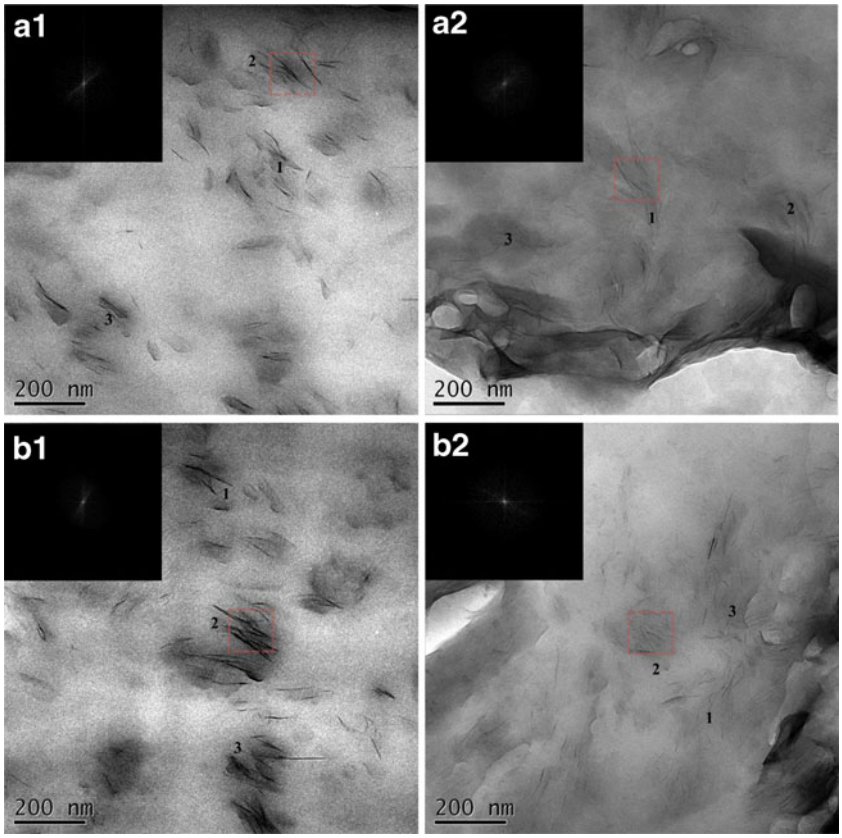

Fig. 6 TEM images and fast Fourier transforms of (a1, a2) BEM-C and (b1, b2) BEM-E

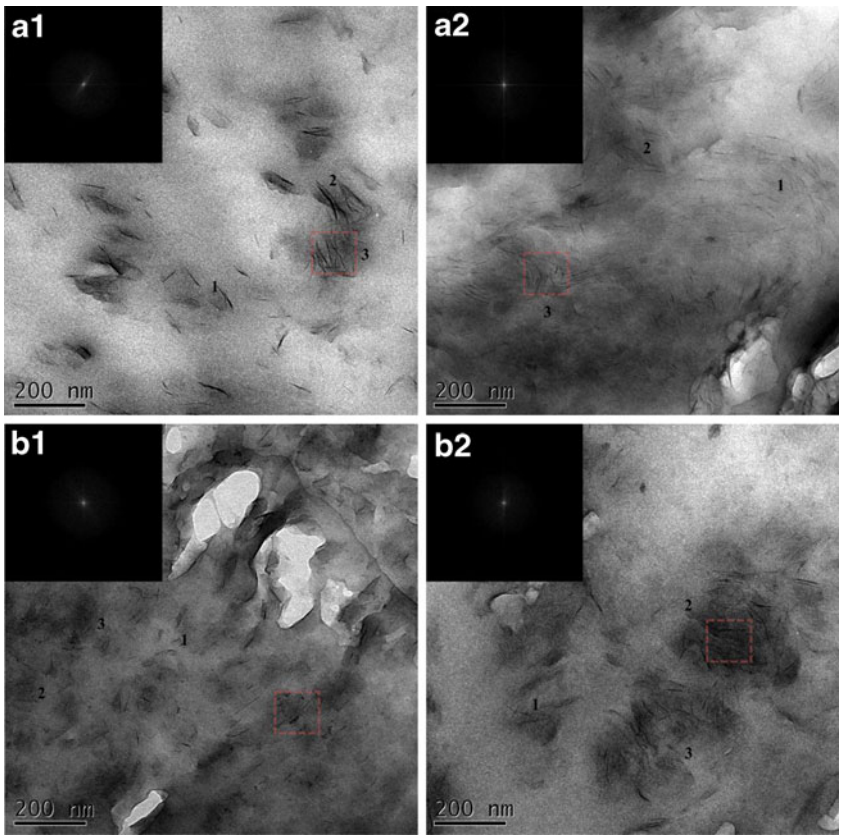

Figure 7 TEM images and fast Fourier transforms of (a1, a2) BEM-F, and (b1, b2) BEM-G

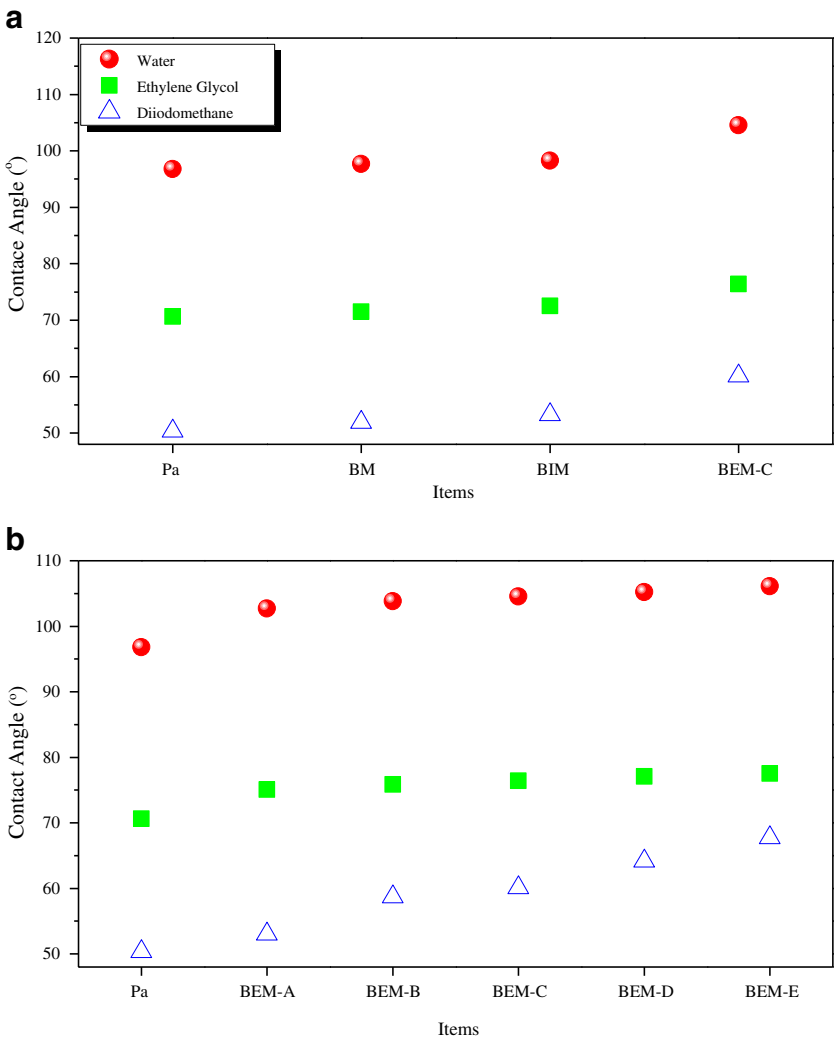

Fig. 8 Contact angle data for (**a**) Pa, BM, BIM, and BEM-C and (**b**) Pa benzoxazine samples containing various contents of Ex-MMT

structures, especially with regard to the degree of dispersion of MMT, In-MMT, and Ex-MMT in the polymeric matrix. The pristine MMT had a lamellar structure [Fig. 1(B)-(a)], In-MMT was an intercalated nanocomposite [Fig. 1(B)-(b)], and Ex-MMT was an exfoliated nanocomposite [Fig. 1(B)-(c)]; therefore, each was dispersed in the polybenzoxazine matrix in a different states. TEM and fast Fourier transform analyses [Fig. 1(B)] clearly revealed the lamellar structures of MMT and In-MMT and the random dispersion of Ex-MMT. The layered morphology implied that the primary building blocks of the nanodomains of MMT consisted of an assembly of many lamellae (lamella multiples), arranged compactly and densely in a certain direction. In-MMT had a similar, or possibly even the same, layered morphology as that of MMT, as revealed in Fig. 1(B)-(b), but the arrangement was not as compact or dense as that of MMT—direct, visible evidence for the intercalation of propargyldimethylstearylammonium bromide into the MMT. Figure 1(B)-(c) reveals that Ex-MMT did not have a lamellar structure; here, the MMT had been exfoliated into nanoparticles, either single sheets or layers, as a result of the click reactions of the cage-like POSS nanoparticles. These single sheets or layers were dispersed randomly and freely in the polymeric matrix. This structure is consistent with the XRD pattern in Fig. 1(A) and confirms that we had successfully prepared the Ex-MMT.

Exfoliated single sheets or layers of MMT can form different dispersion states in a polymeric matrix. Scheme 2(d) reveals single sheets or layers dispersed randomly, freely, and uniformly—a so-called "random dispersion." These single sheets or layers could also gather together to form structures such as islands or stars [Scheme 2(e)]—a so-called "island dispersion." Moreover, the random and island dispersions always appeared together in the form of the mixed dispersion presented in Scheme 2(f). Therefore, the Ex-MMT–based nanocomposites often contained more than one dispersion of the exfoliated single sheets or layers. In Fig. 6, the numbers 1, 2, and 3 represent random, island, and mixed dispersions,

respectively. The BEM samples, including BEM-C [Figs. 6(a1) and (a2)], BEM-E [Figs. 6(b1) and (b2)], BEM-F [Figs. 7(a1) and (a2)] and BEM-G [Figs. 7(b1) and 7(b2)], all featured the dispersions described above. The sizes of the single sheets or layers of MMT in Figs. 1(B) and Fig. 6 were in the range 0.05–1 μm. They comprised some elementary particles (also called "structural units"), which were constituted by some thin solid layers. The size of an elementary particle was approximately 8–10 nm; because the thickness of a thin solid layer was approximately 0.93–1 nm, an elementary particle usually contained about eight thin solid layers. During the intercalation process leading the formation of In-MMT, the exfoliation and click reactions leading to Ex-MMT, and the strong stirring in the preparation of BEM, the MMT was exfoliated into nanoparticles in the form of thin solid layers, elementary particles, or aggregates of the two. In addition, the Ex-MMT nanoparticles and the polybenzoxazine chains underwent an assembly process during the strong stirring used in the preparation of BEM. The different charges of the components led to the formation of ionic bonds between them; this assembly process not only had a further exfoliation effect on the Ex-MMT nanoparticles but also anchored these exfoliated single sheets or layers with polybenzoxazine chains through physical crosslinking. The better the dispersion, the greater the number of physical crosslinking points and, therefore, the stronger the anchoring effect. In addition, the Ex-MMT nanoparticles also interacted with the polybenzoxazine chains indirectly as a result of the latter's compatibility with propargyldimethylstearylammonium bromide. In other words, the structure of MMT, the assembly process, the anchoring effect, and the compatibility of the polymer and intercalator all combined so that the BEM systems possessed structures featuring the random, island, or mixed dispersions displayed in Fig. 6 and Schemes 2(d)–(f).

The pure Pa, BM, BIM, and BEM and the dispersions of MMT, In-MMT, and Ex-MMT in the polybenzoxazine matrix also featured different surface properties, such as surface hydrophobicity. Fig. 8(a) and Table 2 reveal that the surface contact angles of distilled water, EG, and Diio slowly increased upon proceeding from Bz, via BM and BIM, to BEM. The same behavior occurred for the dispersions of MMT, In-MMT, and Ex-MMT in the polybenzoxazine matrix [Fig. 8(b), Table 2]; as the content of Ex-MMT relative to Pa increased in the polybenzoxazine matrix, the surface contact angles tested from these three liquid also increased slowly, but obviously. This polybenzoxazine is a hydrophobic polymer or thermosetting resin that has a low surface energy [15]. After incorporating MMT, In-MMT, or Ex-MMT into the polybenzoxazine matrix, as random, island, or mixed dispersions, the surfaces of the tested samples (10 mm × 8 mm × 2 mm) became much rougher. This roughness caused BM, BIM, and BEM to exhibit large surface contact angles and low surface energies. As revealed in Fig. 8(b) and Table 2 for samples BEM-A to BEM-E, a greater content of Ex-MMT relative to Bz in the polybenzoxazine matrix led to greater roughness on the surfaces of the tested samples, larger surface contact angles, and lower surface energies.

Conclusions

In this study, we introduced Ex-MMT, into a benzoxazine matrix to form exfoliated nanocomposites. The MMT exhibited a completely exfoliated state in the polymeric matrix; this situation differs from that found in previous reports, where it possessed only layered or lamellar structures. The exfoliated single sheets or layers formed random dispersions, island dispersions, or mixed dispersions of the two. Because of the incorporation of Ex-MMT, the value of T_g of the polybenzoxazine improved greatly, as did its surface hydrophobicity.

Acknowledgement This study was supported financially by the National Science Council, Taiwan, Republic of China, under contracts NSC 100-2221-E-110-029-MY3 and NSC 100-2628-E-110-001.

References

1. Sawaryn C, Landfester K, Taden A (2010) Benzoxazine miniemulsions stabilized with polymerizable nonionic benzoxazine surfactants. Macromolecules 43:8933–8941
2. Chernykh A, Agag T, Ishida H (2009) Synthesis of linear polymers containing benzoxazine moieties in the main chain with high molecular design versatility via click reaction. Polymer 50:382–390
3. Tuzun A, Kiskan B, Alemdar N, Erciyes AT, Yagci Y (2010) Benzoxazine containing polyester thermosets with improved adhesion and flexibility. J Polym Sci Part A: Polym Chem 48:4279–4284
4. Aydogan B, Sureka D, Kiskan B, Yagci Y (2010) Polysiloxane-containing benzoxazine moieties in the main chain. J Polym Sci Part A: Polym Chem 48:5156–5162
5. Agag T, Geiger S, Alhassan SM, Qutubuddin S, Ishida H (2010) Low-viscosity polyether-based main-chain benzoxazine polymers: precursors for flexible thermosetting polymers. Macromolecules 43:7122–7127
6. Sawaryn C, Landfester K, Taden A (2011) Benzoxazine miniemulsions stabilized with multifunctional main-chain benzoxazine protective colloids. Macromolecules 44:5650–5658
7. Kiskan B, Colak D, Muftuoglu AE, Cianga I, Yagci Y (2005) Structure of the benzoxazine-functionalized polystyrene. Macromol Rapid Commun 26:819–824
8. Ergin M, Kiskan B, Gacal B, Yagci Y (2007) Thermally curable polystyrene via click chemistry. Macromoleculues 40:4724–4727
9. Nakamura M, Ishida H (2009) Synthesis and properties of new crosslinkable telechelics with benzoxazine moiety at the chain end. Polymer 50:2688–2695
10. Ishida H, Low HY (1997) A Study on the Volumetric Expansion of Benzoxazine-Based Phenolic Resin. Macromolecules 30:1099–1106

11. Ishida H, Allen DJ (1996) Physical and mechanical characterization of near-zero shrinkage polybenzoxazines. J Polym Sci Part B: Polym Phys 34:1019–1030
12. Kiskan B, Ghosh NN, Yagci Y (2011) Polybenzoxazine-based composites as high-performance materials. Polym Int 60:167–177
13. Kanchanasopa M, Yanumet N, Hemvichian K, Ishida H (2001) The effect of polymerization conditions on the density and T_g of bisphenol-A and hexafluoroisopropylidene-cotaining polybenzoxanines. Polym Polym Compos 9:367–375
14. Jin L, Agag T, Ishida H (2010) Bis(benzoxazine-maleimide)s as a novel class of high performance resin: synthesis and properties. Eur Polym J 46:354–363
15. Wang CF, Su YC, Kuo SW, Huang CF, Sheen YC, Chang FC (2006) Low-surface-free-energy materials based on polybenzoxazines. Angew Chem Int Ed 45:2248–2251
16. Kuo SW, Wu YC, Wang CF, Jeong KU (2009) Low Surface Energy Materials through Mediated by Hydrogen Bonding Interaction. J Phys Chem C 113:20666–20673
17. Holly FW, Cope AC (1944) Condensation products of aldehydes and ketones with o-aminobenzyl alcohol and o-hydroxybenzylamine. J Am Chem Soc 66:1875–1879
18. Yang P, Gu Y (2011) Synthesis and curing behavior of a benzoxazine based on phenolphthalein and its high performance polymer. J Polym Res 18:1725–1733
19. Ishida H (2011) In: Ishida H, Agag T (eds.) Handbook of Benzoxazine Resins. Elsevier, Amsterdam, Ch. 1, p. 1–81.
20. Wang CF, Wang YT, Tung PH, Kuo SW, Lin CH, Sheen YC, Chang FC (2006) Fabrication of patterned superhydrophobic polybenzoxazine hybrid surfaces. Langmuir 22:8289–8292
21. Wang CF, Chiou SF, Ko FH, Chen JK, Chou CT, Huang CF, Kuo SW, Chang FC (2007) Polybenzoxazine as a mold-release agent for nanoimprint lithography. Langmuir 23:5868–5871
22. Wang CF, Wang TF, Liao CS, Kuo SW, Lin HC (2011) Using pencil drawing to pattern robust superhydrophobic surfaces to control the mobility of water droplets. J Phys Chem C 115:16495–16500
23. Baqar M, Agag T, Ishida H, Qutubuddin S (2011) Poly(benzoxazine-courethane)s: a new concept for phenolic/urethane copolymers via onepot method. Polymer 52:307–317
24. Su YC, Kuo SW, Yei DR, Xu HY, Chang FC (2003) Thermal properties and hydrogen bonding in polymer blend of polybenzoxazine/poly(*N*-vinyl-2-pyrrolidone). Polymer 44:2187–2191
25. Kuo SW, Liu WC (2010) Synthesis and characterization of a cured epoxy resin with a benzoxazine monomer containing allyl groups. J Appl Polym Sci 117:3121–3127
26. Huang JM, Kuo SW, Lee YJ, Chang FC (2007) Synthesis and characterization of a vinyl-terminated benzoxazine monomer and its blends with poly(ethylene oxide). J Polym Sci Part B: Polym Phys 45:644–653
27. Ishida H, Low HY (1998) Synthesis of benzoxazine functional silane and adhesion properties of glass-fiber-reinforced polybenzoxazine composites. J Appl Polym Sci 69:2559–2567
28. Tragoonwichian S, Yanurnet N, Ishida H (2007) Effect of fiber surface modification on the mechanical properties of sisal fiber-reinforced benzoxazine/epoxy composites based on aliphatic diamine benzoxazine. J Appl Polym Sci 106:2925–2935
29. Kumar KSS, Nair CPR, Ninan KN (2008) Effect of fiber length and composition on mechanical properties of carbon fiber-reinforced polybenzoxazine. Polym Adv Technol 19:895–904
30. Sudo A, Kudoh R, Nakayama H, Arima K, Endo T (2008) Selective formation of poly(N, O-acetal) by polymerization of 1,3-benzoxazine and its main chain rearrangement. Macromolecules 41:9030–9034
31. Agag T, Takeichi T (2008) Preparation and cure behavior of organoclay-modified allyl-functional benzoxazine resin and the properties of their nanocomposites. Polym Compos 29:750–757
32. Fu HK, Huang CF, Kuo SW, Lin HC, Yei DR, Chang FC (2008) Effect of an Organically Modified Nanoclay on Low-Surface-Energy Materials of Polybenzoxazine. Macromol Rapid Commun 29:1216–1220
33. Chozhan CK, Alagar M, Gnanasundaram P (2009) Synthesis and characterization of 1,1-bis(3-methyl-4-hydroxy phenyl)cyclohexane polybenzoxazine–organoclay hybrid nanocomposites. Acta Mater 57:782–794
34. Garea SA, Iovu H, Nicolescu A, Deleanu C (2009) A new strategy for polybenzoxazine–montmorillonite nanocomposites synthesis. Polym Test 28:338–347
35. Chen Q, Xu RW, Yu DS (2006) Multiwalled Carbon Nanotube/Polybenzoxazine Nanocomposites: Preparation, Characterization and Properties. Polymer 47:7711–7719
36. Huang JM, Tsai MF, Yang SJ, Chiu WM (2011) Preparation and thermal properties of multiwalled carbon nanotube/polybenzoxazine nanocomposites. J Appl Polym Sci 122:1898–1904
37. Lee YJ, Kuo SW, Su YC, Chen JK, Tu CW, Chang FC (2004) Syntheses, thermal properties, and phase morphologies of novel benzoxazines functionalized with polyhedral oligomeric silsesquioxane (POSS) nanocomposites. Polymer 45:6321–6331
38. Lee YJ, Huang JM, Kuo SW, Chen JK, Chang FC (2005) Synthesis and characterizations of a vinyl-terminated benzoxazine monomer and its blending with polyhedral oligomeric silsesquioxane (POSS). Polymer 46:2320–2330
39. Chandramohan A, Devaraju S, Vengatesan MR, Alagar M (2012) "Octakis(dimethylsiloxypropylglycidylether)silsesquioxane (OG-POSS) reinforced 1,1-bis(3-methyl-4-hydroxymethyl) cyclohexane based polybenzoxazine nanocomposites". J Polym Res 19:9903
40. Liu YH, Zheng SX (2006) Inorganic–organic nanocomposites of polybenzoxazine with octa(propylglycidyl ether) polyhedral oligomeric silsesquioxane. J Polym Sci Part A Polym Chem 44:1168–1181
41. Huang JM, Kuo SW, Huang HJ, Wang YX, Chen YT (2009) Preparation of VB-a/POSS hybrid monomer and its polymerization of polybenzoxazine/POSS hybrid nanocomposites. J Appl Polym Sci 111:628–634
42. Wu YC, Kuo SW (2010) Synthesis and characterization of polyhedral oligomeric silsesquioxane (POSS) with multifunctional benzoxazine groups through click chemistry. Polymer 51:3948–3955
43. Huang KW, Kuo SW (2011) Inorganic–Organic Nanocomposites of Vinyl-terminated Benzoxazine with Octa(propylglycidyl ether) Polyhedral Oligomeric Silsesquioxane. Polym Compos 32:1086–1094
44. Kuo SW, Chang FC (2011) POSS related polymer nanocomposites. Prog Polym Sci 36:1649–1696
45. Chen Q, Xu R, Zhang J, Yu D (2005) Polyhedral Oligomeric Silsesquioxane (POSS) Nanoscale Reinforcement of Thermosetting Resin from Benzoxazine and Bisoxazoline. Macromol Rapid Commun 26:1878–1882
46. Chou CH, Hsu SL, Dinakaran K, Chiu MY, Wei KH (2005) Synthesis and Characterization of Luminescent Polyfluorenes Incorporating Side-Chain-Tethered Polyhedral Oligomeric Silsesquioxane Units. Macromolecules 38:745–751
47. Chou CH, Hsu SL, Yeh SW, Wang HS, Wei KH. Enhanced Luminance and Thermal Properties of Poly(phenylenevinylene) Copolymer Presenting Side-Chain-Tethered Silsesquioxane Units. *Macromolecules* 38: 9117-9123
48. Tseng MC, Liu YL (2010) Preparation, morphology, and ultra-low dielectric constants of benzoxazine-based polymers/polyhedral oligomeric silsesquioxane (POSS) nanocomposites. Polymer 51:5567–5575
49. Cui HW, Kuo SW (2012) Using a polyhedral oligomeric silsesquioxane surfactant and click chemistry to exfoliate montmorillonite. RSC Adv 2:12148–12152

50. Huang KW, Kuo SW (2010) High performance polybenzoxazine nanocomposites containing multifunctional polyhedral oligomeric silsesquioxane (POSS) with allyl groups. Macromol Chem Phys 211:2301–2311
51. Lin YC, Kuo SW (2011) Self-assembly and secondary structures of linear polypeptides tethered to polyhedral oligomeric silsesquioxane nanoparticle through click chemistry. J Polym Sci Part A: Polym Chem 49:2127–2137
52. Lin YC, Kuo SW (2012) Synthesis, self-assembly and secondary structures of linear polypeptides graft to polyhedral oligomeric silsesqu ioxane in the side chain through click chemistry. Polym Chem 3:162–171
53. Hu WH, Huang KW, Kuo SW (2012) Heteronucleobase-functionalized benzoxazine: synthesis, thermal properties, and self-assembled structure formed through multiple hydrogen bonding interactions. Polym Chem 3:1546–1554